LES STUDY OF INFLUENCE OF OBSTACLES ON TURBULENT PREMIXED FLAMES IN A SMALL SCALE VENTED CHAMBERS

S.R. Gubba[a], S.S. Ibrahim[b] and W. Malalasekera[a]
S.S.Ibrahim@Lboro.ac.uk
[a]Wolfson School of Mechanical and Manufacturing Engineering, [b]Department of Aerospace and Automotive Engineering, Loughborough University, Loughborough, LE11 3TU, UK

Abstract
The LES study reported in this paper presents the influence of number and position of the obstacles on turbulent premixed flames. LES simulations have been carried out for a stagnant, stoichiometric propane/air mixture, ignited from rest in a small laboratory scale, vented chamber, capable of rearranging into various configurations based on number and position of baffle plates. The novelty of the present study is two folded. First is the application of novel dynamic flame surface density (DFSD) model to account the sub-grid scale (SGS) chemical reaction rate in LES. Second is the arrangement of these configurations into four families, which facilitate a qualitative comparison with available experimental measurements. The concept of families also offers to understand the flame-flow interactions and the impact of number and position of the baffles with respect to ignition origin.

Introduction

Large Eddy Simulations (LES) are now accepted as a feasible computational tool to study transient turbulent premixed flames despite added computational cost. Several recent works [1-5] confirms the high fidelity nature of LES in predicting key characteristics of turbulent combustion. LES is being attracted by numerical modellers due the fact that, large eddies above a cut-off length scale are resolved and the small ones are modelled using SGS models. Also the cost and accuracy of the solutions lies between the DNS and RANS techniques. In spite of numerical and computational advancements, crucial issue to the advancement of LES lies in the development of adequate SGS models, which are capable of representing combustion over a wide range of flow and combustion conditions. This remains a key challenge, facing the turbulent combustion community.

In LES, as the reaction zone thickness of the premixed flame to be resolved is thin, with a characteristic length scale much smaller than a typical LES filter width, an appropriate SGS model is vital to account for the SGS chemical reactions. The work presented in this paper is continuation from the previous LES studies [6] and the recent progress made in development of a dynamic flame surface density (DFSD) model [7-8] to account the SGS chemical reaction rate by the same authors. Our earlier studies [7] using DFSD model based on laminar flamelets seems to be promising in predicting key characteristics of the propagating turbulent premixed flames with inbuilt solid obstacles. However, the novel DFSD model was studied for very few configurations [8], which limit our understanding on its application.

In the present work, the novel DFSD model is used to simulate transient turbulent premixed flames, propagating in a small vented chamber having various solid obstacles. One main objective of the present study is forming various configurations by rearranging the

baffles strategically in the path of propagating turbulent flame. The novel experimental test facility [9] used in this study to compare LES simulations offers this capability, which formulates various flow configurations having a range of turbulent intensities. Furthermore, these configurations can be arranged into families based on number and position of the solid baffles, where effects of generated turbulence on combustion can be studied. The concept of the families also offers to understand the flame-flow interactions and the impact of number and position of the baffles with respect to ignition origin.

LES simulations have been carried using a grid independent resolution for eight configurations, which are then arranged into four families. Numerical predictions are compared with the available experimental data in order to validate the novel DFSD model for all these flow configurations. Results are discussed highlighting the merits and drawbacks of the model while construing flame dynamics and behaviour in various families.

Test Cases

The novel experimental chamber used in this study was developed by The University of Sydney, Australia. Construction details of the test chamber are described in our earlier publications [6]. This chamber can accommodated maximum of 3 baffle plates at stations S1, S2, S3 located at equidistance and a solid square obstacle at about 96 mm from down stream of ignition end. Eight configurations rendered using this test chamber is considered in the present study as shown in Figure 1. Table 1 provides details of the families classified based on number and position of the baffles plates. It should be noted here that the configuration 0 with no baffles is not been included in any of the families. However, this configuration is useful in understanding the flame propagation and the dynamics within the chamber.

Numerical Modelling

Transient calculations of deflagrating flames in vented chambers shown in Figure 1 are carried out using large eddy simulation (LES) methodology. In LES, modelling the mean chemical reaction rate in turbulent premixed flames is very challenging due to its non-linear relation with chemical and thermodynamic states, and often characterized by propagating thin reaction layers thinner than the smallest turbulent scales. In the present simulations, the SGS chemical reaction rate is accounted by using the novel DFSD model [2, 7 & 8]. Brief details of the model are given here as details are presented elsewhere [7].

The mean SGS chemical reaction rate $\overline{\dot{\omega}}_c$ in reaction progress variable equation is modelled by following the laminar flamelet approach as:

$$\overline{\dot{\omega}}_c = \rho_u u_L \overline{\Sigma} \tag{1}$$

where ρ_u is the density of unburned mixture, u_L is the laminar burning velocity, and $\overline{\Sigma}$ is the flame surface density. The term, mean filtered flame surface density $\overline{\Sigma} = \overline{|\nabla c|}$ (in Eq. 1), can be split into two terms as resolved and unresolved:

$$\overline{\Sigma} = \overline{|\nabla c|} = \underbrace{\prod\left(\overline{c}, \overline{\Delta}\right)}_{\text{Resolved}} + \underbrace{f\left(\overline{c}, \overline{\Delta}, \prod\left(\overline{c}, \overline{\Delta}\right)\right)}_{\text{Unresolved}} \tag{2}$$

where c is the mean reaction progress variable, $\overline{\Delta}$ is the filter width and *Cs* is the model coefficient. An over-bar describes application of the spatial filter, while the hat (ˆ) denotes test filter application. The resolved term in the above equation is evaluated using the following expression:

$$\lambda = \overline{\Sigma} - \prod\left(\overline{c}, \overline{\Delta}\right) = \overline{|\nabla c|} - \prod\left(\overline{c}, \overline{\Delta}\right) \tag{3}$$

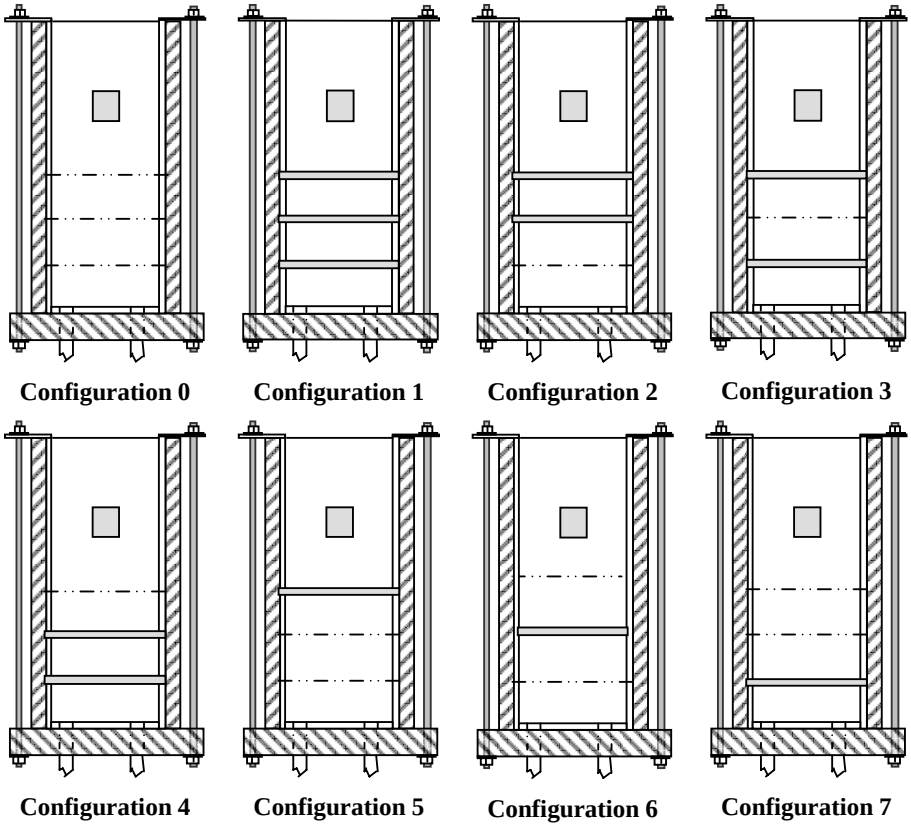

***Figure 1**. Illustration of various combustion configurations employed (Not to scale).*

Table 1. Classification of Families.

Family	Description		Overpressure (mbar)		Incidence time (ms)	
		Configuration	Exp	LES	Exp	LES
1	Baffles are progressively increased and kept farthest from ignition end	5	79.93	71.20	13.46	13.34
		2	122.07	106.92	11.92	11.88
		1	138.28	124.60	10.30	10.98
2	Baffles are progressively increased from ignition source	7	45.00*	58.45	11.00*	12.50
		4	77.15	60.26	9.79	10.82
		1	138.28	124.60	10.30	10.98
3	Two baffles are positioned at different stations of the chamber	2	122.07	106.92	11.92	11.88
		3	86.91	82.22	11.63	11.99
		4	77.15	60.26	9.79	10.82
4	Only one baffle positioned at different stations of the chamber	5	79.93	71.20	13.46	13.34
		6	63.00*	65.21	10.00*	12.12
		7	45.00*	58.45	11.00*	12.50
Base Configuration		0	34.00	36.60	13.50	13.50

* Indicated pressure and time using rich mixture [12].

Defining γ as a ratio of test filter to grid filter, i.e. $\langle\Delta\rangle/\bar{\Delta}$, such that the test filter $\langle\Delta\rangle$ is greater than the grid filter $\bar{\Delta}$. Applying the test filter to flame surface density (Eq. 2) leads to:

$$\langle\bar{\Sigma}\rangle = \langle|\overline{\nabla c}|\rangle = \underbrace{\prod(\langle\bar{c}\rangle,\langle\bar{\Delta}\rangle)}_{\text{Resolved@testfilter}} + \underbrace{\left[\langle|\overline{\nabla c}|\rangle - \prod(\langle\bar{c}\rangle,\langle\bar{\Delta}\rangle)\right]}_{\text{Unresolved@testfilter}} \tag{4}$$

From the above equation, unresolved flame surface density contribution at the test filter level can be written as:

$$\Lambda = \left[\langle|\overline{\nabla c}|\rangle - \prod(\langle\bar{c}\rangle,\langle\bar{\Delta}\rangle)\right] \tag{5}$$

Assuming the sub-grid scale contribution of unresolved flame surface density at test filter is the same as that at grid filter and relating λ and Λ by using Germano identity [10]:

$$\begin{aligned}\Lambda - \langle\lambda\rangle &= \left[\langle|\overline{\nabla c}|\rangle - \prod(\langle\bar{c}\rangle,\langle\bar{\Delta}\rangle)\right] - \left[\langle|\overline{\nabla c}|\rangle - \langle\prod(\bar{c},\bar{\Delta})\rangle\right] \\ \Lambda - \langle\lambda\rangle &= \left[\langle\prod(\bar{c},\bar{\Delta})\rangle - \prod(\langle\bar{c}\rangle,\langle\bar{\Delta}\rangle)\right]\end{aligned} \tag{6}$$

The sub-grid scale flame surface density contribution from the above equation can be added to the resolved flame surface density (Eq. 4) with a model coefficient *Cs* in order to obtain total flame surface density. Hence the flame surface density can be expressed as:

$$\bar{\Sigma} = \prod(\bar{c},\bar{\Delta}) + Cs\left[\langle\prod(\bar{c},\bar{\Delta})\rangle - \prod(\langle\bar{c}\rangle,\langle\bar{\Delta}\rangle)\right] \tag{7}$$

The model coefficient *Cs* in above equation is dynamically obtained by identifying sub-grid scale flame surface as a fractal surface [4] as follows:

$$Cs = \frac{1}{1-\gamma^{2-D}}\left[\left(\frac{\bar{\Delta}}{\delta_c}\right)^{D-2} - 1\right] \tag{8}$$

where δ_c is the lower cut-off scale, γ is the ratio of test filter to grid filter and D is the fractal dimension, calculated dynamically [4].

The numerical model described above, has been implemented in an in-house LES code PUFFIN [11]. Other mathematical details of the code are not described here as available in our earlier publications [6 & 8]. LES results presented in the next section are carried out using a grid independent resolution of 90 x 90 x 336 (2.7 million) in 3 dimensional space.

Results and Discussions

Results from the LES simulations of stagnant, stoichiometric propane/air deflagrating flames over solid obstacles are presented and discussed in this section. A novel DFSD model [4 & 7] to account the SGS chemical reaction rate is used to model premixed combustion in the vented chambers shown in Figure 1. Eight flow configurations considered here are classified into four families as detailed in Table 1 and analysed for flame dynamics, structure and other combustion characteristics. Each baffle plate and the solid square obstacle used inside the chamber are aimed to generate turbulence by disrupting the flame propagation with a blockage ratio of 40% and 25% respectively. Primary objective of the present work is the application of DFSD model in predicting the turbulent premixed flame dynamics in a wide range of flow configurations. Secondly, influence of the position of individual baffle plate in generating overpressure, due to the interactions with deflagrating flames, with respect to the origin of ignition is examined.

Flame Characteristics: Configuration 0

Configuration 0 has no baffles except a solid square obstacle running through out the chamber. Since, baffles are not presented in this chamber, the flame took longer to encounter solid obstacle and to reach blow-down stage, than in any other configuration which are due to

discuss in next sections. Time series of overpressure and flame position from LES simulations are briefly shown against experimental measurements in Figure 2. The overpressure trend from LES is very encouraging, as it is in excellent agreement from ignition to blow-down with measurements, including the time of pressure rise at about 11.5 ms, slope of pressure rise, peak pressure and its incidence time at 13.5 ms. Also, Figure 2 confirms the LES predictions of peak overpressure of 36.6 mbar at 13.5 ms against experiments measurement of 34 mbar at 13.5 ms, which is slightly over-predicted by 7.6%. It is also evident from Figure 2 that the pressure reflections, once the main flame left the chamber are also in good agreement with experiments. Similarly, the flame position shown in Figure 2 confirms this observation with an exact match of, up to peak overpressure and thereafter with a slight, but considerable deviation.

Figure 3 shows sequence of flame front images from LES (reaction rate contours) and experiments (false colourised images extracted from high speed video). It is evident from these images, that the LES simulations are capable to reproduce turbulent flame structure very accurately at various stages. For instance at 12 ms, the flame shape (finger shape) and its approach towards square obstacle can be immediately noticed. Similarly, at 13.5 ms (peak overpressure incidence) LES captured same shape of experimental image i.e. flame engulfs upstream of square obstacle by trapping certain amount of unburnt mixture, which can be seen to burnt before 14.5 ms. However, there is some unburnt mixture trapped in recirculation zone, which will burn after main flame left the chamber, which is causing pressure reflections at a later stages.

From Figure 3 (a) it can be noticed that the turbulent flame thickness predicted by LES is about 1 to 2 grid width and the formation of wrinkles can be clearly noticed once flame starts hitting the square obstacle. However, these flame wrinkles cannot be clearly seen in experimental video images (Figure 3 (b)), as they are global images taken from the outside of the chamber.

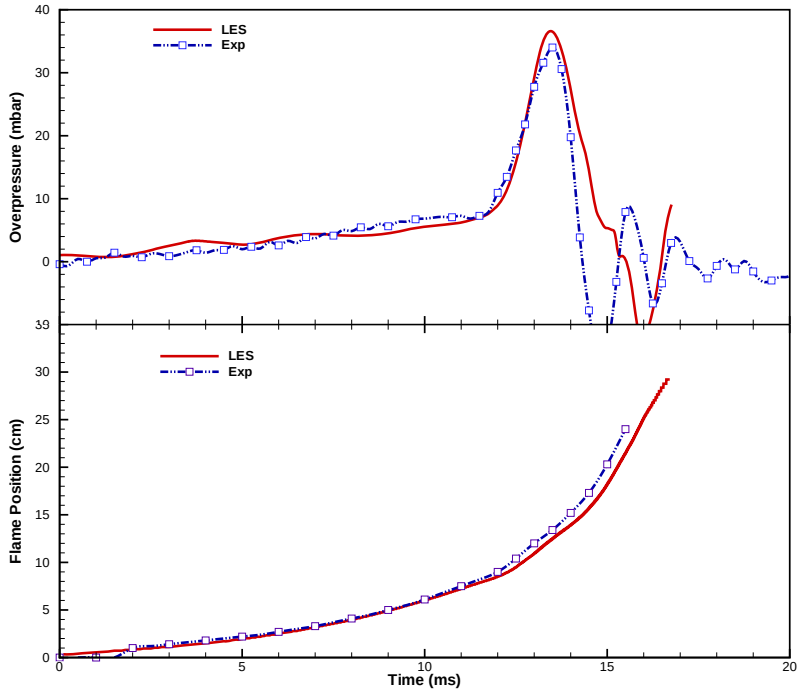

***Figure 2**. Time histories of overpressure and flame position for configuration 0.*

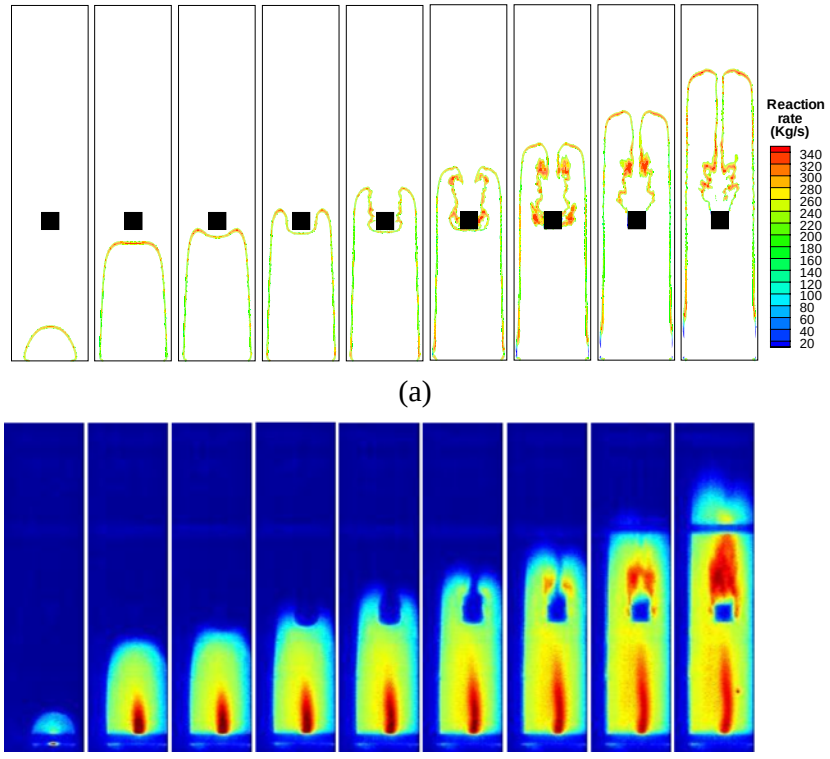

***Figure 3**. Series of flame images at 6.0, 12.0, 12.5, 13.0, 13.5, 14.0, 14.5, 15.0, 15.5 ms respectively after ignition (a) LES (b) Experimental video images (false colourised).*

Figure 4 shows the measured mean axial, radial and their RMS velocity information against LES predictions. It should be noted here that the measurements have been carried at the middle of the chamber (*x*-axis) and half way up the side of the square obstacle i.e. 102 mm from the base (*z*-axis) and 16 mm from the central axis (*y*-axis) using LDV technique. Experimental axial (W) and radial (V) velocity measurements shown in Figure 4 are the coordinates of the average polynomial fitted to the ensemble averaged velocity data from over 50 repeatable, individual experiments. Accordingly, RMS fluctuations of W and V are calculated from the variance between a polynomial fitted to the mean velocity data.

In case of LES, the data is available from only one simulation and moreover, the flame is of totally unsteady nature, and therefore unable to obtain ensemble averaged velocity information. Hence, the only alternative choice to calculate/obtain RMS of velocity is by choosing a suitable bin size. From LES calculations, it is identified that there exist large number of data points (~100 to 500) for every one millisecond of flow due to the limitation of CFL number. Therefore, a bin size of 0.25 ms has been chosen to extract average and its variance of velocity profile at 102 mm from ignition base and 16 mm from the central axis without loosing unsteady information. Averaged and RMS velocities are calculated as:

$$\overline{x} = \frac{\Sigma x_i}{n} \tag{9}$$

$$\text{RMS} = \left(\frac{\Sigma (x_n - \overline{x})^2}{n} \right) \tag{10}$$

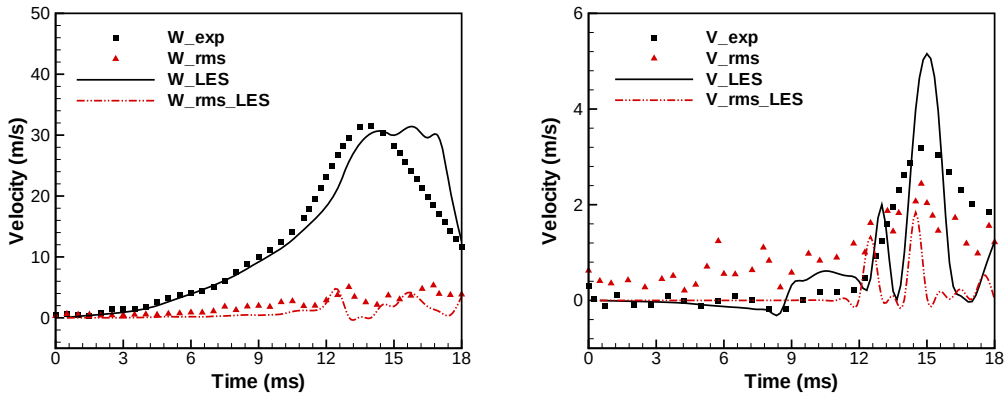

(a) (b)

Figure 4*. Time histories of velocities and their RMS fluctuations for configuration 0 at (a) axial (b) radial velocity.*

It is evident from Figure 4(a) that the maximum axial velocity has reached 32 m/s at approximately 14.5 ms as obtained from both experiments and LES. Velocity mean and RMS profiles of the LES are in excellent agreement up to approximately 15 ms and in fair agreement with experimental measurements thereafter. The RMS fluctuations in Figure 4(a) provide very good information of the turbulence levels at various stages of the flame. It can be seen that, the rate of increase in turbulence and its decay is fairly well predicted at peak pressure incidence i.e. 13.5 ms and during blow-down phase.

Considering the radial velocity mean and its RMS from Figure 4(b), peaks of the mean and RMS velocities from LES are matching with experiments. It can also be noticed that, the experimental radial RMS values (red triangles) during early stages of the flame propagation (before 12 ms) measured are higher than ensemble averaged velocity (black squares) and this phenomenon is highly questionable from experimental point of view itself. Nevertheless, LES predictions of radial RMS fluctuations are found to follow the same trend of LES velocity profile.

Flame Characteristics: Family 1

Family 1 consists of configurations 5-2-1 with progressively increasing the number of baffles from one to three and positioned farthest from ignition bottom as detailed in Table 1. The time histories of overpressure and flame position from LES and experiments are plotted as shown in Figure 5 (a) & (b) respectively. It is evident from Figure 5(a) that the overpressure trend is in excellent agreement, however, slightly under-predicted. Nevertheless, comparing the LES simulations presented in our earlier publication using simple FSD model [6], these predictions are very good in terms of magnitude, trend and timing, which were main drawbacks identified while using the FSD model. This is mainly due to the novel DFSD model employed, which is efficient in calculating unresolved flame surface density. Figure 5(a) also highlights the impact of number of baffles and their position with respect to distance from the ignition bottom. The time elapsed in reaching the first baffle from the ignition bottom and increase in the steepness of pressure gradient due to the generated turbulence can be easily noticed. Similarly, the flame position shown in Figure 5(b) is also predicted very well except in case of configuration 2. In case of experiments, the flame position is extracted from high speed video images by locating the farthest location of the flame front from ignition bottom end. From LES calculations, the flame position is obtained by locating the farthest location of the leading edge of the flame front from the bottom end (defined here as the most down stream location of the flame, where c = 0.5 from the ignition point).

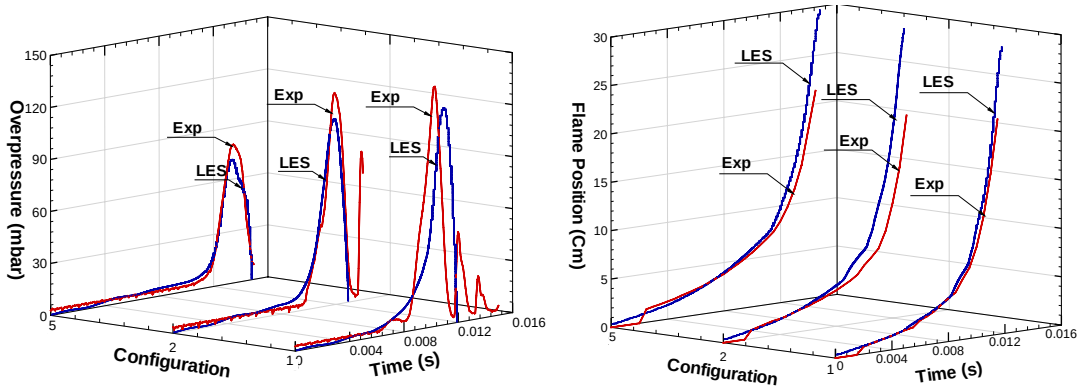

(a) (b)

Figure 5. *Comparison of predicted and measured time traces of Family 1 (a) overpressure (b) flame position.*

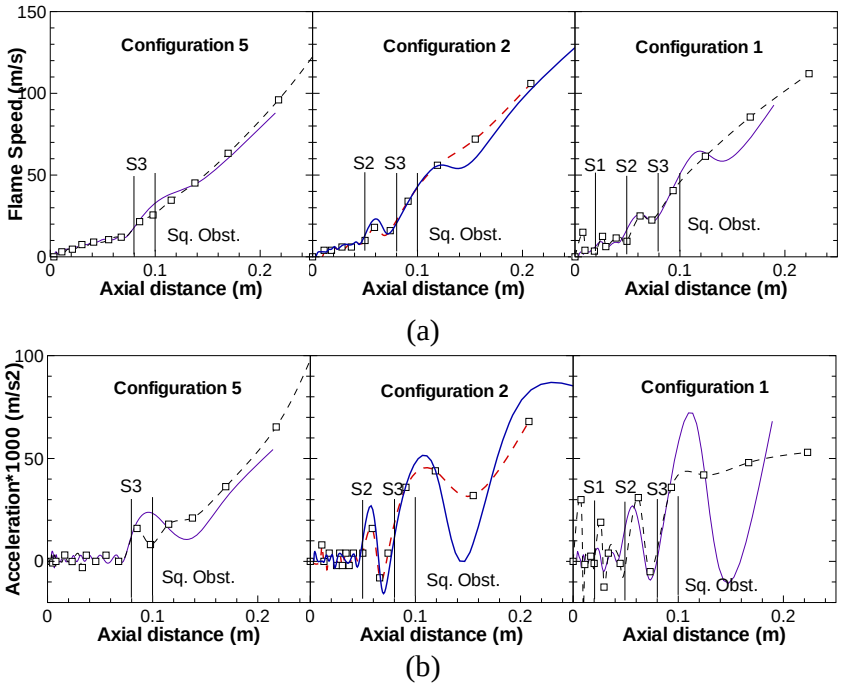

(a)

(b)

Figure 6*. Comparisons between predicted (Solid line) and measured (Dashed lines with square symbols) (a) flame speed (b) flame acceleration vs. axial distance. The location of baffle stations (S1, S2 and S3) and the square solid obstacle are shown.*

Figure 6 (a) & (b) shows flame speed and acceleration respectively from LES and experiments derived from flame images. It can be noticed that the flame speed and acceleration from LES are in good agreement with experimental measurements, except when the flame is located downstream of square obstacle in blow-down region. One main reason for this is due to the limitation in resolution of experimental measurements. Within blow-down region, the flow conditions are highly turbulent and flame propagates faster with approximately about 80-100 m/s in this family.

Figure 7 presents cut-view of LES predicted reaction rate contours, showing flame structure at 6.0, 8.0, 10.0, 11.5 and 12.0 ms after ignitions for whole family. This facilitates qualitative and quantitative comparison of flame position and its structure at any given time

within this family. For instance at 8.0 ms from Figure 7 (a) & (b), which illustrates the finger shaped flame structure, which is generally expected in chambers having l/d ratio greater than 3. Figure 7(b) at 11.5 and 12.0 ms shows a clear picture of entrapment of unburnt fuel/air mixture around solid square obstacle within recirculation zone. The pockets or traps in case of configuration 1 in Figure 7(c) at 10.0 and 11.5 ms are clearly noticeable. Similarly, Figure 7(c) at 11.5 and 12.0 ms shows the consumption of trapped mixture, once the main flame left the chamber. Figure 7 also quantifies the influence of baffles on overpressure and turbulence generation through flame structure.

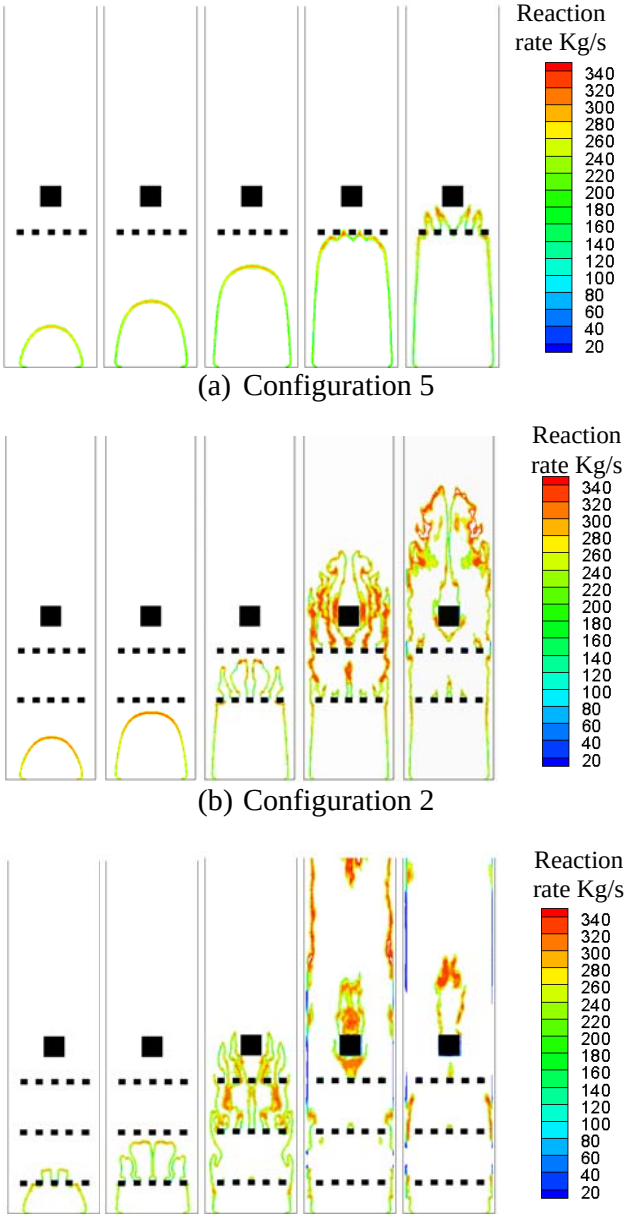

Figure 7*. Predicted flame structure from three configurations at 6, 8, 10, 11.5 and 12.0 ms after ignition.*

In order to facilitate further discussion, magnitude and incidence time of overpressure for four families are plotted as shown in Figure 8. It is evident from Figure 8(a) that, as

expected the overpressure generated is higher in the case of configuration 1 since it has 3 baffles with an earlier incidence time and lower in configuration 5 due to one baffle with a later incidence time. It is very interesting to note that the incidence time in this family maintains a linear relation while overpressure has a non-linear relation as seen in Figure 8(a). The magnitude of the overpressure is increased 50% and 75% due to the addition of one and two baffles in configuration 2 & 1 respectively, when compared to the overpressure of configuration 5, which has one baffle at S3. However, incidence time is decreased by 11.5% and 23% in configuration 2 &1 respectively, inline with configuration 5. One reason for the non-linear relation of overpressure might be due to the position of baffles from the ignition source, even though they have the same blockage ratio. This will be further discussed in the next section.

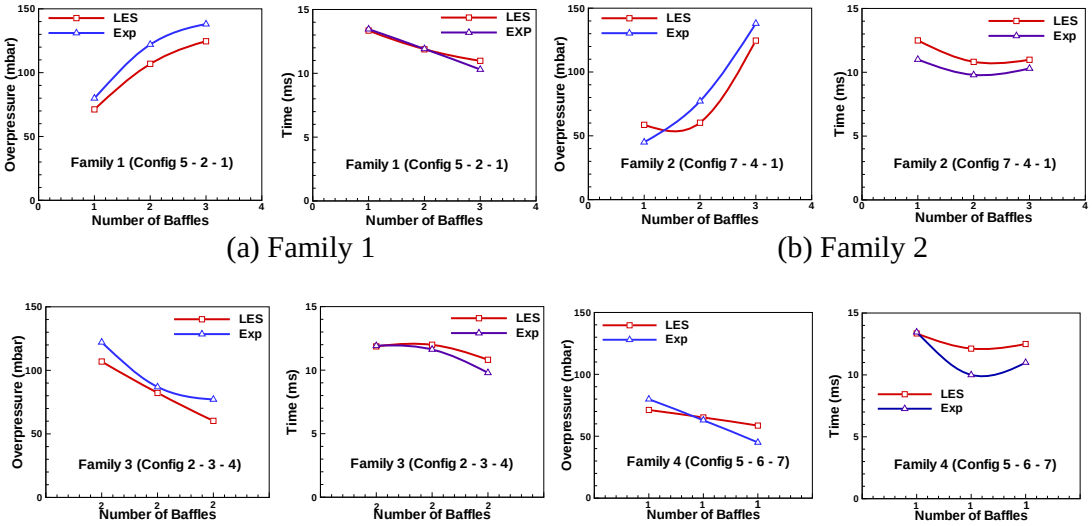

(a) Family 1 (b) Family 2

(c) Family 3 (d) Family 4

Figure 8*. Variation of peak overpressure and its time of incidence compared from LES vs. Experiments for four families.*

Flame Characteristics: Family 2

Family 2 consists of 7-4-1 configurations with progressively increasing baffles from 1 to 3, from ignition end as detailed in Table 1. Since the details of configuration 7 and 4 are being discussed in next sections, this section is kept to minimal to avoid repetition. The overpressure and its incidence times for the whole family can be seen from Figure 8(b). It is evident that both overpressure and the time are maintaining non-linear relation in this Family. The overpressure has increased 71% and 206% in configuration 4 and 1 compared to the measured overpressure in configuration 7. However, the incidence times are decreased by about 10-15%. Combining the results of family 1 and 2 in Figure 8 (a) & (b) facilitates to derive mainly the following points.

- Although the baffle plate in configuration 7 & 4 has same blockage capacity, less overpressure is generated in configuration 7, which is due to the position of baffle from the ignition bottom. Similarly, configuration 4 & 2 have two baffles with same blockage capacity and generated less overpressure than in configuration 2. This observation confirms that the blockage with same capacity, nearer to the ignition source would

generate less overpressure at an earlier time, when compared with the blockage positioned far from ignition source. In addition, it can also be observed that the timing of peak pressure in configuration 7 & 4 are less when compared to configuration 5 & 2.

- Although the overpressure increases with blockage ratio, the rate of this increase from configurations 4 to 1 and 2 to 1 is not the same, as observed in Figure 8 (a) & (b) respectively.

Flame characteristics: Family 3

Family 3 has three configurations i.e. 2-3-4 with two baffle plates at different stations and a solid square obstacle at a fixed position. Figure 9 (a) & (b) shows characteristic comparison of overpressure and flame position respectively for three configurations, from experimental measurements and LES simulations. It is evident from Figure 9(a) that the rate of pressure rise and its trend including first hump are predicted well except for configuration 4, where the computed rate of increase of pressure is slower than measurements indicating a faster decay of turbulence between the second baffle plate and the square obstacle. Figure 9 (b) outlines the flame position in configuration 3 as fully overlapped and a slightly faster propagation rate across the chamber in configurations 2 and 4. It should be noticed here that this phenomenon is only observed in the last few milliseconds of propagation where the flame is experiencing the highest levels of turbulence.

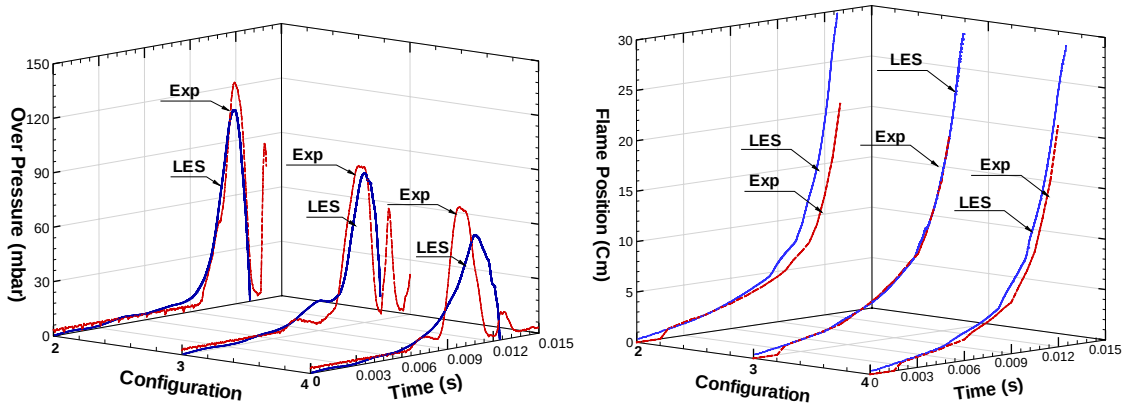

(a) (b)

Figure 9. *Comparison of predicted and measured time traces of Family 3 (a) overpressure (b) flame position.*

Figure 10 shows comparison between experimental measurements and numerical predictions of flame speed and acceleration. Figure 10 also shows the position of baffle plates and the solid square obstacle to identify the influence of the obstacles. Highest flame speed and acceleration are recorded at the square obstacle in configuration 2 than other two configurations. It is also interesting to note that, in configuration 4, the slowdown in flame speed and acceleration between the second baffle plate and the square obstacle due to relatively longer distance compared to other configurations in this Family.

Figures 11 present the predicted flame structure from the reaction rate contours at strategic instants i.e. 6, 8, 10, 11.5 and 12.0 ms after ignition. In addition, axial, radial velocities and their RMS fluctuation from LES are compared with LDV measurements in these configurations, as shown in Figure 12. This facilitates the analysis of the flame position, structure and flow behaviour at any chosen time. The time taken by the flame front to reach

solid square obstacle, to generate maximum overpressure and venting of the flame are strongly influence by this initial laminar behaviour of the flame. For instance at 6 ms, the flame is jetting out of the baffle plate at S1 in configuration 3 and 4. In configuration 2 at this instance, the flame is smooth and laminar relatively with a lower speed, which mainly caused take longer time to reach square obstacle in this case.

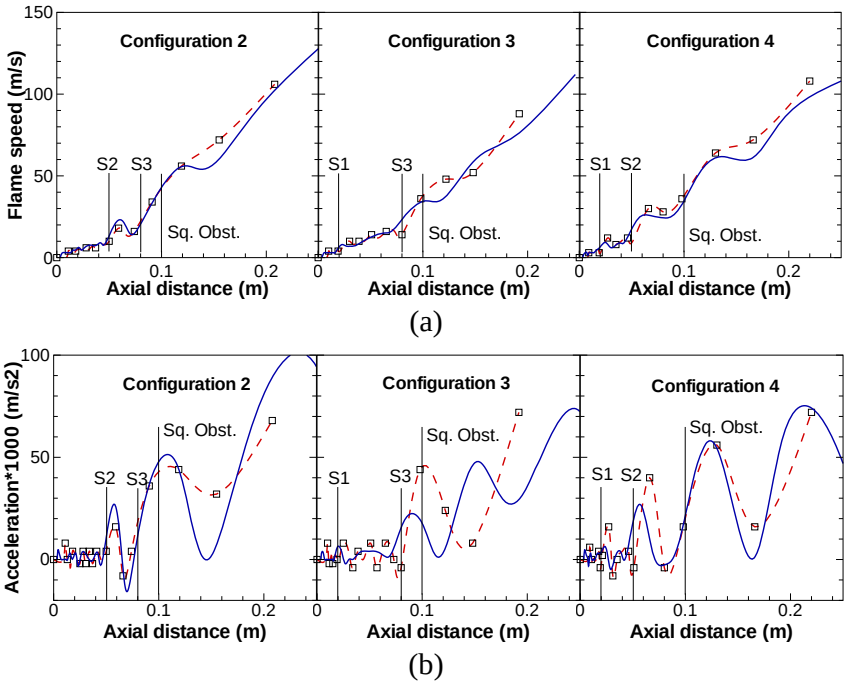

***Figure 10**. Comparisons between predicted (Solid line) and measured (Dashed lines with square symbols) (a) flame speed (b) flame acceleration vs. axial distance. The location of baffle stations (S1, S2 and S3) and the square solid obstacle are shown.*

As seen from Figure 12 (b) & (c), the RMS of axial velocity is computed as 2 m/s for configurations 3 & 4. However, the flame is found to be hemi-spherical and laminar with a negligible RMS fluctuation (< 0.2 m/s) in configuration 2 at 6 ms as seen in Figure 12 (a). Similarly, considering the reaction rate contours at 10 ms, the flame is about to interact with baffle plate at S3 with totally different flame structure and respective RMS fluctuations of 4 and 5 m/s from configuration 2 and 3. The flame in configuration 4 found to be more turbulent at 10 ms with RMS velocity of 8 m/s (at its peak in this configuration) and about to interact with solid square obstacle. Hence, the differences in flame position, flame front structure and the degree of wrinkles are found to be directly related to the axial location of baffles with respect to the origin of ignition.

It is very interesting to note that using two baffles plates with a solid square obstacle having same blockage capacity in all the configurations, the recorded and predicted overpressure is maximum in configuration 2 and minimum in configuration 4 as shown in Figure 8 (c). Interestingly, LES predictions are showing a linear relation for generated overpressure and not by experiments. However, the predicted overpressure is very much in-line with experiments. It is also evident from Figure 12 that, the flame exits the chamber faster in configuration 4 than in configuration 2. However, configuration 3 is in between the other two configurations in case of maximum overpressure and flame arrival time in the chamber. In case of configuration 2, though the flame has laminar nature until it reaches the first baffle plates at S2, quickly turn out to be highly turbulent due to jetting and contortion of

the flame through the repeated obstacles. In this configuration the turbulent fluctuations are found to be progressively increasing and reach a maximum of 9 m/s at 11.5 ms. The laminar nature of flame front during the initial stages i.e. up to 8 ms has caused longer blow down time from the chamber at later stages. It should be noted, that the baffles and square obstacle in configuration 2 are almost all evenly spaced from bottom of ignition centre. While in configuration 4, flame found to be highly turbulent during initial stages followed by a faster decay at later stage.

It should be noted in configuration 3 that, once the flame is distorted after reaching first baffle, flame front is slightly wrinkled with a higher surface area. However, re-laminarisation (reduction in speed and turbulence levels) of the flame between S1 and S3 results in approaching the square obstacle at a later stage compared to configuration 4. This is also evident from the computed RMS fluctuations at 10 ms as 5 and 8 m/s and at 11.5 ms as 5 and 7 m/s respectively in configuration 3 and 4.

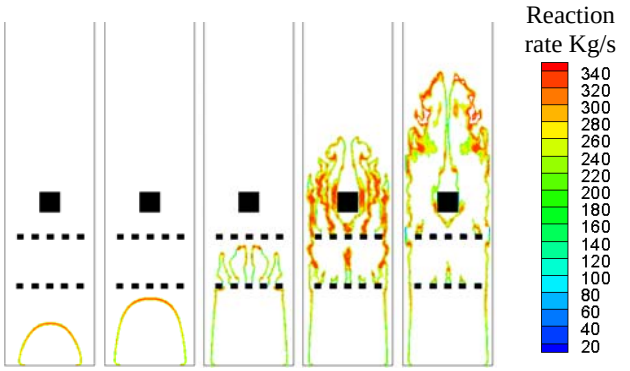

(a) Configuration 2

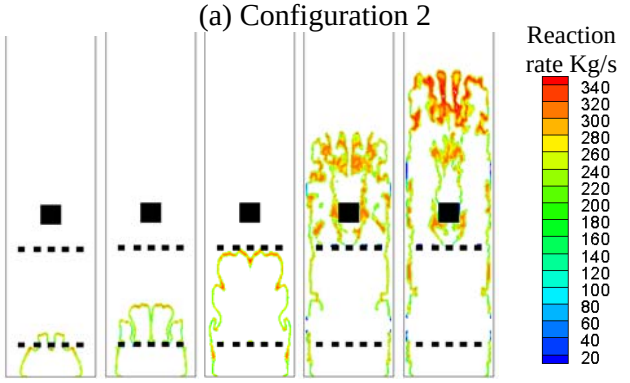

(b) Configuration 3

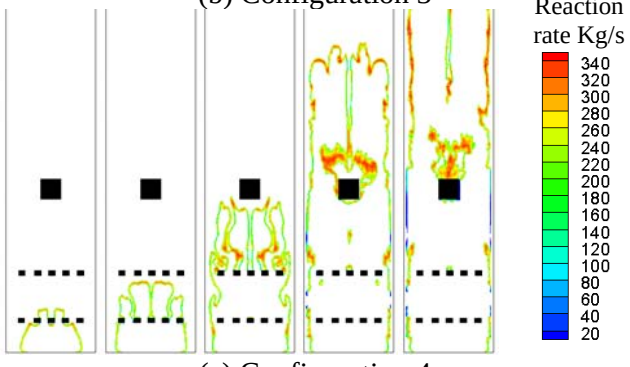

(c) Configuration 4

Figure 11. *Predicted flame structure from three configurations at 6, 8, 10, 11.5 and 12.0 ms after ignition. (a) Configuration 2 (b) Configuration 3 (c) Configuration 4*

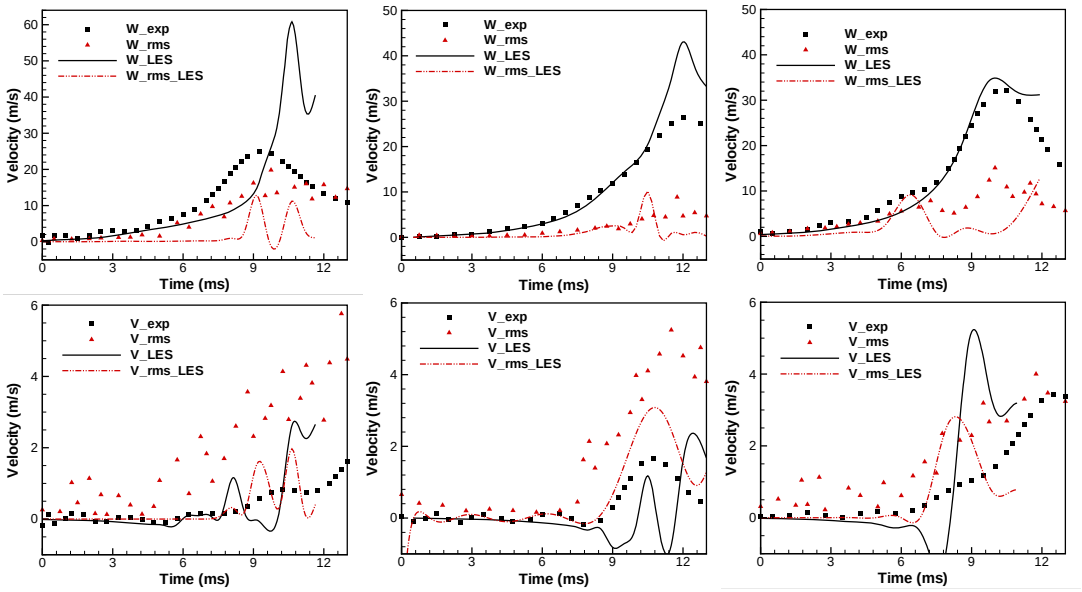

***Figure 12**. Axial and radial velocity, time histories and their RMS fluctuations of various configurations in Family 2. (a) Configuration 2 (S2 & S3) (b) Configuration 3 (S1 & S3) and (c) Configuration 4 (S1 & S2).*

Flame Characteristics: Family 4

Family 4 consists of 5-6-7 configurations with only one baffle positioned at different stations and a square obstacle. Experimental measurements for configuration 6 and 7 are not available to compare. However, indicative overpressure and incident time from work of Hall et al. [12] using rich mixture having equivalence ratio 1.1 are used in Figure 8 (d). The time histories of overpressure for three configurations are shown in Figure 13 (a). As discussed earlier in case of other families, the novel DFSD formulation is very successful in predicting turbulent premixed flames. It is evident from Figure 13 (a) that the time traces of overpressure from LES for configuration 5 are very closely matching with the experimental measurements. It can be clearly seen that every stage of flame propagation including interacting with baffle plate and solid obstacle are reproduced very well. The time of peak overpressure occurrence is perfectly matched. However, the magnitude is slightly under predicted. It is also evident that DFSD model is successful in predicting pressure gradient at various stages of the flame propagation.

Figure 13 (b) & (c) presents flame position, speed against time and speed against axial distance of the chamber. Evidently it can be observed that the flame position and speed with time and flame speed with position in Figure 13(d) for configuration 5 are predicted very well. Reaction rate contours from LES, at five important instants are plotted in Figure 14 to study the flame-obstacle interactions in this family. The instants chosen are 6, 8, 10, 12 and 13 ms in all configurations, which generally matches with flame evolution, interaction with baffle plate, interactions with square obstacle, formation of recirculation zone and blow-down of flame from chamber.

The reaction rate contours at 6 and 8 ms provide a greater deal in giving information about the nature of flames. At these instants, configuration 5 & 6 has perfectly identical structure, shape with same flame thickness and the reaction rate. Since configuration 7 has a baffle plate at S1, flame has interacted and jetted through the baffle, which eventually changes

the flame shape. However, the flame position at 8 ms in configuration 7 is almost all equal to the flame position in other two configurations (see Figure 13(d)) and just started to propagate at higher speed. At 10 ms, the flame in configuration 7 has higher surface area to consume more mixture due to its interaction with the baffle plate at 6ms. By this time in configuration 6, the flame has evolved through baffle slits and started to form individual flame kernels. However, the flame in configuration 5 is still smooth and had a finger shaped structure propagating in axial direction proportional to gas expansion ratio.

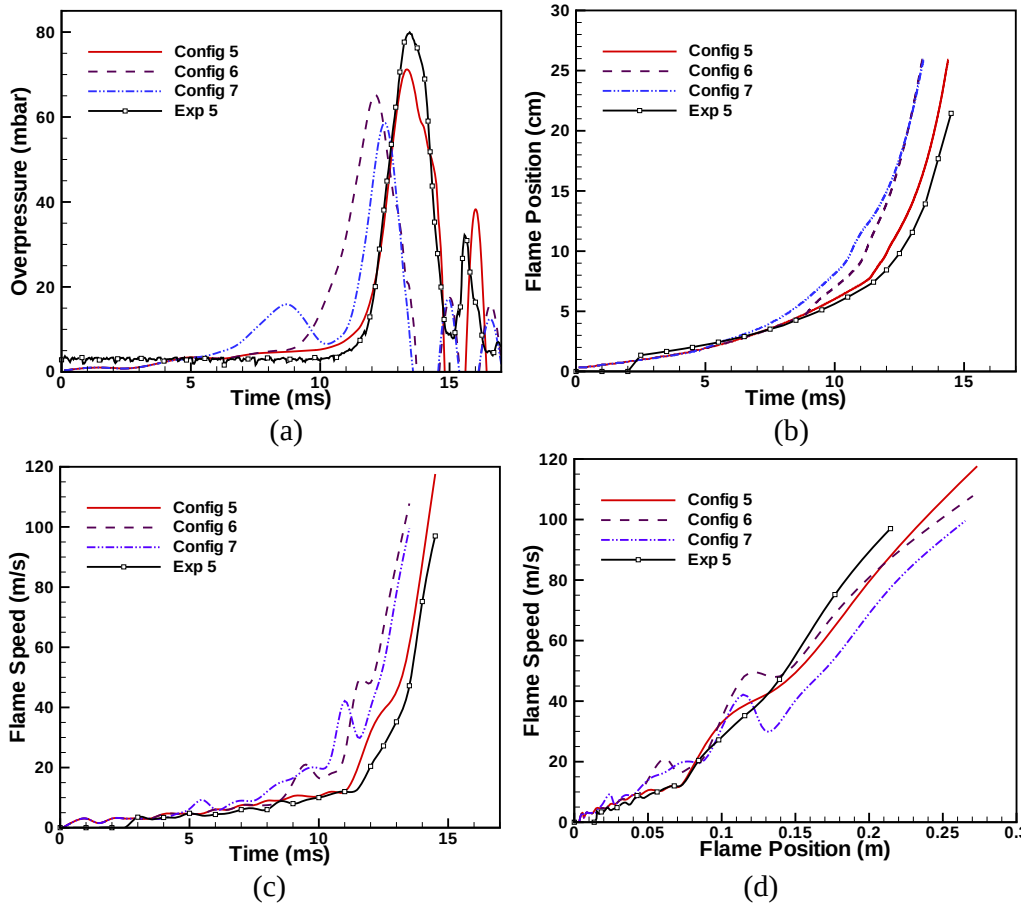

Figure 13. *Flame characteristics of Family 4 (a) Time traces of overpressure (b) Time traces of flame position (c) Time traces of flame speed and (d) Flame speed with axial location of chamber.*

Reaction rate contours at 12 ms are very interesting and delineating information about the flame entrapment around square obstacle. By comparing configuration 6 and 7 at this instant, it is evident that, configuration 7 has more surface area with smoother outer flame structure and wrinkled inner flame structure. The inner flame structure is responsible for trapping of unburned mixture. The flame has smoother inner structure in configuration 6 and engulfs lesser amount of mixture compared to configuration 7. Also, some flame islands can be observed in the case of configuration 6, which is responsible for slightly higher overpressure at any given time compared to configuration 7.

Comparing reaction rate contour at 13 ms from configuration 5 with contours at 12 ms of configuration 6 & 7, enhances the idea of how, individual flow configuration traps unburned mixture around obstacles. It can be clearly observed that the mixture trapped in case of

configuration 5 is very less compared to other configurations and the flame spreads within the boundary layer region around the square obstacle. One reason for this might be the gap between baffle and square obstacle, which is affecting the turbulence intensity of the flow within the chamber. At 13 ms from configuration 6 & 7, it can be observed the flame positions overlaps again and the both configurations shows similar nature of the flame i.e. consuming trapped mixture downstream of square obstacles and overlapping of the two branches of flame separated due to obstacles.

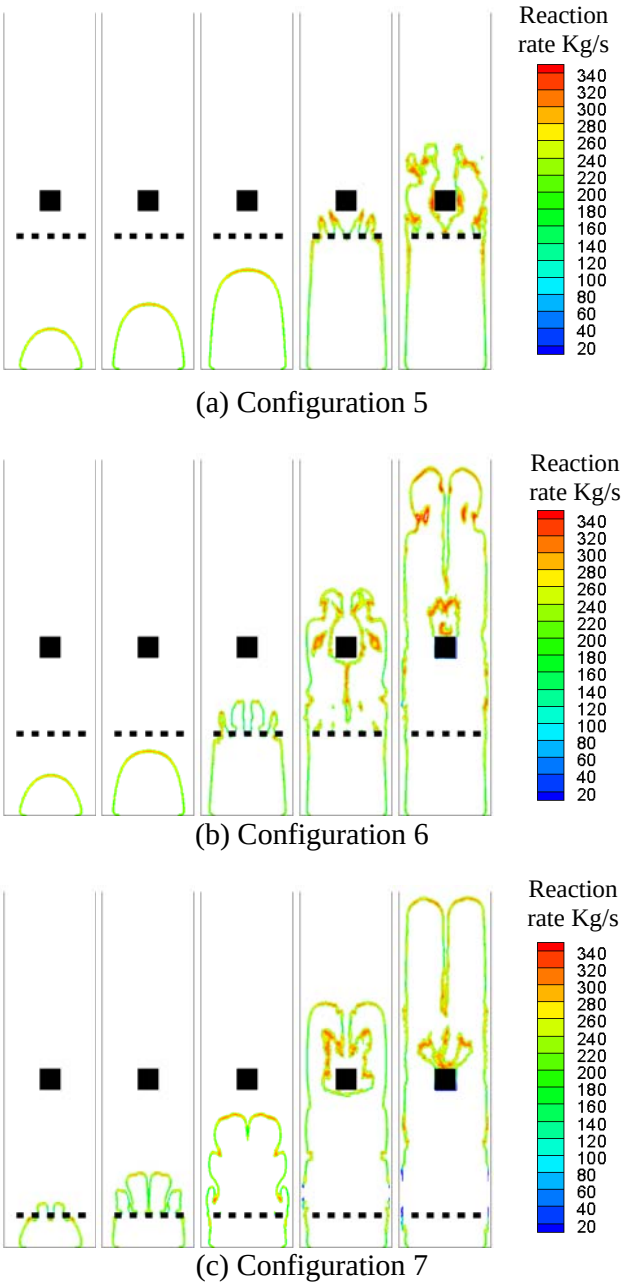

Figure 14. *Snapshots of reaction rate contours at 6.0, 8.0, 10.0, 12.0 and 13 ms in various configurations.*

Figure 8(d) shows peak overpressure and their incidence times from LES and experiments (indicative pressure and time only for configuration 6 and 7). It is very interesting to know that in this family, overpressure from LES is maintaining linear relation. The experimental overpressure is also maintaining linear relation and however with a different slope. The incidence time in case of LES and Experiments are not maintaining linear relation as such and LES incidence times are showing slight over-prediction.

It is very interesting to know that the configuration 5, having a baffle at S3 (away from ignition bottom) has recorded higher overpressure of 71.2 mbar at 13.35 ms. Configuration 7 having one baffle at S1, near to ignition bottom has recorded 58.6 mbar at 12.5 ms. Configuration 6 having one baffle at S2 has recorded overpressure of 65.2 mbar at 12.12 ms in between other two. This observation evidently confirms the observation made in case of Family 3 i.e. farther the baffles to ignition centre, higher the overpressure at later stage. Closure the baffles to the ignition source or end, lesser the magnitude of the overpressure at an earlier stage.

Conclusions

LES simulations have been carried out for propagating turbulent premixed flames in eight flow configurations using novel DFSD model for stoichiometric, stagnant propane/air mixture. The flow configurations have been classified into 4 families based on number and position of baffles. This paper mainly concludes the following points/observations.

- The novel DFSD model is successful in predicting the flame behavior, structure; position and other characteristics in agreement with experimental measurements. Although the overpressure-time trend is in excellent agreement, it is identified that slightly under-predicted for some configurations. This drawback can be probably rectified using additional sub-models for flame curvature and strain in turbulent premixed flames.
- This investigation demonstrates the comparison of LES predictions with experimental measurements and the effects of placing multiple obstacles at various locations in the path of the turbulent propagating premixed flames. As expected, it concludes that the increase in blockage ratio increases the overpressure, however, with same blockage ratio, the position of solid obstruction with respect to each other and ignition end has a significant impact on the magnitude of the overpressure and spatial flame structure.
- It is identified that the overpressure representing the generated energy in any individual configuration, is directly proportional to the number of baffles plates used in this study. The flame speed and the development of the reaction zone are clearly dependent on the number of obstacle used and their blockage ratio.
- Extensive flame-flow interactions occur as the flame propagates past the baffle plate and the solid obstructions leading to the formation of disconnected flame islands with higher burning rates. The flame progressively accelerates as it travels through the various stages of the chamber. Turbulent burning velocities of about 12 to 14 m/s were achieved at the open end of the chamber. However there are no evidences to prove the presence of flame quenching due to elongation and stretching in the present study. This may be due to the small volume of the chamber used in this study.
- Large separation between the solid baffle plates allows sufficient residence time for turbulence decay causing flow re-laminarisation and hence lowering overpressures with a much smooth flame fronts.
- Higher pressure gradient develops along the length of the chamber with more number of baffles or obstacles.

- It is identified that the trapped unburnt mixtures up and down stream of obstacles are consumed once the main flame leaves the chamber leading to subsequent oscillations in pressure.
- The location of the obstacles with respect to the ignition source has a direct impact on the overpressure and the structure of the reaction zone. Extending the distance between the baffles or between baffles and the downstream obstacle, allows turbulence to re-laminarise. Although with same blockage capacity, this phenomenon leads lower overpressure and less distortion in the reaction zone. This new finding highlights the transient nature of the interaction between the propagating flame front and the local condition of the flow field.

References

[1] Charlette, F., Meneveau, C. and Veynante, D., "A power-law flame wrinkling model for LES of premixed turbulent combustion Part II: dynamic formulation", *Combustion and Flame,* 131: (1-2), 181-197 (2002).

[2] Knikker, R., Veynante, D. and Meneveau, C., "A dynamic flame surface density model for large eddy simulation of turbulent premixed combustion", *Physics of Fluids,* 16: (11), L91-L94 (2004).

[3] Fureby, C., Pitsch, H., Lipatnikov and Hawkes, E., "A fractal flame-wrinkling large eddy simulation model for premixed turbulent combustion", *Proceedings of the Combustion Institute,* 30: (1), 593-601 (2005).

[4] Masri, A.R., Ibrahim, S.S. and Cadwallader, B.J., "Measurements and large eddy simulation of propagating premixed flames", *Experimental Thermal and Fluid Science,* 30: (7), 687-702 (2006).

[5] Pitsch, H., "Large-eddy simulation of turbulent combustion", *Annual Review of Fluid Mechanics,* 38, 453-482 (2006).

[6] Gubba, S.R., Ibrahim, S.S., Malalasekera, W., Masri, A.R., “LES modelling of premixed deflagrating flames in vented explosion chamber with a series of solid obstructions”, *Comb. Sci. Tech.*, 10 (180), 1936-1955, (2008).

[7] Gubba, S.R., Ibrahim, S.S., Malalasekera, W., Masri, A.R., “LES of premixed turbulent combustion using a dynamic flame surface density model”, To appear in *Flow, Turbulence and Combustion*.

[8] S.S. Ibrahim, S.R. Gubba, AR Masri and W Malalasekera., “Calculations of explosion deflagrating flames using a dynamic flame surface density model”, *Journal of Loss and Prevention in Process Industries*, (In Press, Corrected Proof available at: http://dx.doi.org/10.1016/j.jlp.2008.05.006).

[9] Kent, J. E., Masri, A. R., and Starner, S. H., “A new chamber to study premixed flame propagation past repeated obstacles”, Paper presented at the *5Th Asia-Pacific Conference on Combustion,* The University of Adelaide, Adelaide, Australia (2005).

[10] Germano, M., Piomelli, U., Moin, P. and Cabot, W.H., "A dynamic subgrid-scale eddy viscosity model", *Physics of Fluids A: Fluid Dynamics,* 3: (7), 1760-1765 (1991).

[11] Kirkpatrick, M. P., Armfield, S. W., Masri, A. R., & Ibrahim, S. S., “Large eddy simulation of a propagating turbulent premixed flame”, *Flow, Turbulence and Combustion,* 70: (1-4), 1-19 (2003).

[12] Hall, R., Masri, A.R., Yaroshchyk, P. and Ibrahim, S.S., "Effects of position and frequency of obstacles on turbulent premixed propagating flames", *Combustion and Flame,* 156: 439-446 (2009).